Optical and Quantum Electronics **18** *(1986) 381–401*

S_0–S_n Two-photon absorption dynamics of rhodamine dyes

P. SPERBER, A. PENZKOFER
Naturwissenschaftliche Fakultät II – Physik, Universität Regensburg, 8400 Regensburg, FRG

Received 23 May; accepted 11 July 1986

The intensity-dependent transmission of picosecond ruby laser pulses of different duration through methanolic and ethanolic solutions of rhodamine B and rhodamine 6G is analysed. The transmission is affected by S_0–S_n two-photon absorption, by stimulated emission at the pump-laser frequency, by amplified spontaneous emission and by excited-state absorption. Various parameters involving the two-photon absorption dynamics are determined by comparing experiments with numerical simulations.

1. Introduction

The two-photon absorption of dye solutions at elevated laser intensities has been studied previously by fluorescence observation [1–14]. Two-photon absorption cross-sections $\sigma^{(2)}$ were determined for various dyes [1–7]. The fluorescence induced by two-photon absorption has found wide application in picosecond-pulse duration measurements [8]. Dye-laser pumping by two-photon absorption was achieved [9, 10]. Deviations of the two-photon excited-fluorescence signal from the expected quadratic dependence on pump-laser intensity has been observed indicating the simultaneous action of additional spectroscopic effects (excited-state absorption, stimulated emission, etc.) [2, 3, 11–15].

In this paper the two-photon absorption dynamics of dyes is investigated by transmission measurements. The dyes rhodamine 6G and rhodamine B in methanolic and ethanolic solution are studied. The pump laser is a mode-locked ruby laser. The relaxation of the excited molecules involves radiationless decay, fluorescence emission, excited-state absorption, stimulated emission at pump-laser frequency, amplified spontaneous emission and fluorescence reabsorption. The dynamics are simulated with a realistic level scheme.

2. Theory

A realistic level diagram for the S_0–S_n two-photon-absorption dynamics is shown in Fig. 1. The two-photon absorption excites molecules from the S_0 ground state (region 1) to a higher excited singlet state, S_{n1} ($n1 \geqslant 2$, level 2). The molecules in higher excited singlet states relax rapidly to the first excited singlet state, S_1 (level 3). Direct relaxation from higher excited singlet states to the ground state, S_0, is neglected. Before relaxation to the S_1 state, excited-state absorption may elevate some molecules from S_{n1} to S_{n4} (level 4). From the first excited singlet state, S_1 (level 3), the molecules return to the ground state by spontaneous emission (indicated by transition to level 7), by radiationless decay, by stimulated emission at the pump-laser frequency, ν_L (transition to level 8), and by amplified spontaneous emission (transition to level 9, frequency ν_{ASE}). Within the S_0 state the population of levels 7, 8, 9 thermalize with vibrational relaxation time τ_v [16–18]. The fluorescence emission within the S_0–S_1 absorption region is partially reabsorbed (transition 7 → 3). The pump laser at frequency ν_L and the generated amplified spontaneous emission signal at frequency ν_{ASE} suffer excited-state absorption from S_1 to S_{n2} and S_{n3}, respectively. The intersystem crossing from

0306–8919/86 $03.00 + .12

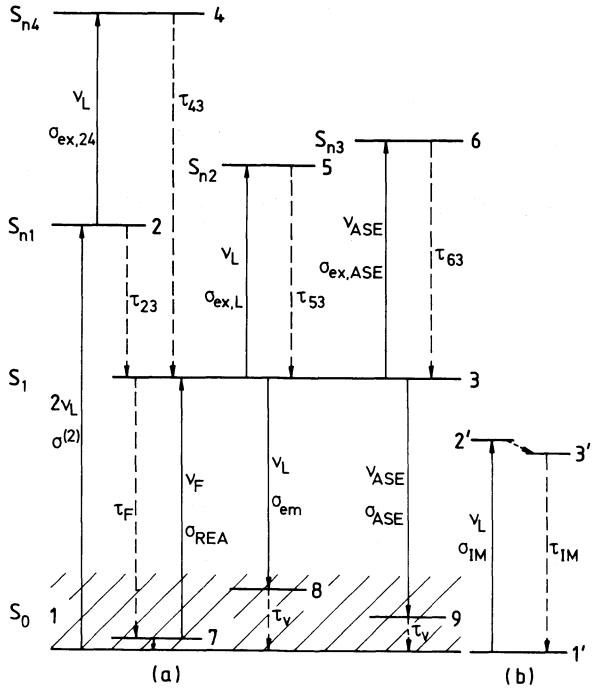

Figure 1 Level system.

singlet states to triplet states is neglected because the transmission behaviour of picosecond pulses has been studied and on a picosecond time-scale the transfer to triplet states is negligibly small (for rhodamine 6G, rate $k_{S_1T} = 4.2 \times 10^5\,s^{-1}$ [19], for rhodamine B, $k_{S_1T} = 1.7 \times 10^6\,s^{-1}$ [20]). The extremely small fraction of molecules in thermally populated vibrational states or inhomogeneously shifted states within the S_0 band are able to populate directly the S_1 state (transition $8 \rightarrow 3$) [21, 22] with absorption cross-section σ_{em}. Laser light scattering (cross-section σ_{SCA}) and impurity absorption (σ_{IM}) may contribute to the single-photon absorption at the laser frequency. The impurity absorption may be bleached at high intensities. The S_0–T singlet–triplet absorption is negligibly small for the rhodamine dyes investigated and is not included in the level scheme (T_1–S_0 radiative lifetimes: $\tau_{ph} = 1.5\,s$ for rhodamine 6G and $\tau_{ph} = 1.6\,s$ for rhodamine B, solvent ethanol [23]).

The rhodamine 6G and rhodamine B molecules in methanol and ethanol are treated as single species. For the dye concentration used of $0.04\,mol\,dm^{-3}$, a fraction of about 8% of the molecules are statistically so close together that they interact mutually (closely spaced pairs) [24]. They have a double peaked S_0–S_1 absorption spectrum [24] and act as quenching centres in the concentration quenching of the fluorescence lifetime [25]. The S_0–S_n ($n \geqslant 2$) absorption of these closely spaced pairs is found to be the same as the monomer absorption. The influence of the fraction of mutually interacting dye molecules is only taken into account by a reduction of the S_1-state fluorescence lifetime.

The transitions in the level system of Fig. 1 are described by the following system of rate equations. The transformation $t' = t - nz/c$ is used, with n the refractive index and c the vacuum light velocity. Only isotropic single-photon and two-photon absorption cross-sections are considered, i.e. absorption anisotropy of two-photon [3, 26] and of single photon processes [27, 28] is neglected. The system of equations reads

$$\frac{\partial N_1}{\partial t'} = -\frac{\sigma^{(2)}(N_1 - N_2)}{2(h\nu_L)^2} I_L^2 + \frac{\sigma_{em}(N_3 - N_8)}{h\nu_L} I_L + \frac{\sigma_{ASE}(N_3 - N_9)}{h\nu_{ASE}} I_{ASE} + \frac{1}{\tau_F} N_3 - \sigma_{REA}(N_7 - N_3) \frac{I_{REA}}{h\nu_F} \tag{1}$$

$$\frac{\partial N_2}{\partial t'} = \frac{\sigma^{(2)}(N_1 - N_2)}{2(h\nu_L)^2} I_L^2 - \frac{\sigma_{ex,24}(N_2 - N_4)}{h\nu_L} I_L - \frac{1}{\tau_{23}} N_2 \tag{2}$$

$$\frac{\partial N_3}{\partial t'} = \frac{1}{\tau_{23}} N_2 - \frac{\sigma_{ex,L}(N_3 - N_5)}{h\nu_L} I_L - \frac{\sigma_{ex,ASE}(N_3 - N_6)}{h\nu_{ASE}} I_{ASE} - \frac{\sigma_{em}(N_3 - N_8)}{h\nu_L} I_L$$
$$- \frac{\sigma_{ASE}(N_3 - N_9)}{h\nu_{ASE}} I_{ASE} + \sigma_{REA}(N_7 - N_3) \frac{I_{REA}}{h\nu_F} + \frac{1}{\tau_{53}} N_5 + \frac{1}{\tau_{63}} N_6 - \frac{1}{\tau_F} N_3 + \frac{1}{\tau_{43}} N_4 \tag{3}$$

$$\frac{\partial N_4}{\partial t'} = \frac{\sigma_{ex,24}(N_2 - N_4)}{h\nu_L} I_L - \frac{1}{\tau_{43}} N_4 \tag{4}$$

$$\frac{\partial N_5}{\partial t'} = \frac{\sigma_{ex,L}(N_3 - N_5)}{h\nu_L} I_L - \frac{1}{\tau_{53}} N_5 \tag{5}$$

$$\frac{\partial N_6}{\partial t'} = \frac{\sigma_{ex,ASE}(N_3 - N_6)}{h\nu_{ASE}} I_{ASE} - \frac{1}{\tau_{63}} N_6 \tag{6}$$

$$\frac{\partial N_7}{\partial t'} = \frac{e_{A,REA}}{\tau_{rad}} N_3 - \sigma_{REA}(N_7 - N_3) \frac{I_{REA}}{h\nu_F} - \frac{N_7 - \varrho_7 N_1}{\tau_v} \tag{7}$$

$$\frac{\partial N_8}{\partial t'} = \frac{\sigma_{em}(N_3 - N_8)}{h\nu_L} I_L - \frac{N_8 - \varrho_8 N_1}{\tau_v} \tag{8}$$

$$\frac{\partial N_9}{\partial t'} = \frac{e_{T,ASE}}{\tau_{rad}} N_3 + \frac{\sigma_{ASE}(N_3 - N_9)}{h\nu_{ASE}} I_{ASE} - \frac{N_9 - \varrho_9 N_1}{\tau_v} \tag{9}$$

$$\frac{\partial N_{1'}}{\partial t'} = - \frac{\sigma_{IM} N_{1'}}{h\nu_L} I_L + \frac{1}{\tau_{IM}} N_{3'} \tag{10}$$

$$\frac{\partial N_{3'}}{\partial t'} = \frac{\sigma_{IM} N_{1'}}{h\nu_L} I_L - \frac{1}{\tau_{IM}} N_{3'} \tag{11}$$

$$\frac{\partial I_L}{\partial z} = - \frac{\sigma^{(2)}(N_1 - N_2)}{h\nu_L} I_L^2 - \sigma_{ex,24}(N_2 - N_4) I_L - \sigma_{ex,L}(N_3 - N_5) I_L + \sigma_{em}(N_3 - N_8) I_L$$
$$- \sigma_{SCA} N_0 I_L - \sigma_{IM} N_{1'} I_L \tag{12}$$

$$\frac{\partial I_{ASE}}{\partial z} = \frac{e_{T,ASE}}{\tau_{rad}} N_3 h\nu_{ASE} \frac{r_0^2}{4l^2} + \sigma_{ASE}(N_3 - N_9) I_{ASE} - \sigma_{ex,ASE}(N_3 - N_6) I_{ASE} - \sigma_{SCA} N_0 I_{ASE} \tag{13}$$

$$\frac{\partial I_{REA}}{\partial z} = \frac{e_{A,REA}}{\tau_{rad}} N_3 h\nu_F \frac{r_0^2}{4l^2} - \sigma_{REA}(N_7 - N_3) I_{REA} - \sigma_{SCA} N_0 I_{REA} \tag{14}$$

The initial conditions for the number density (dimension, cm^{-3}) of the level populations are $N_1(t' = -\infty, r, z) = N_0$, $N_2(-\infty) = N_3(-\infty) = N_4(-\infty) = N_5(-\infty) = N_6(-\infty) = 0$, $N_7(-\infty) = \varrho_7 N_0$, $N_8(-\infty) = \varrho_8 N_0$, and $N_9(-\infty) = \varrho_9 N_0$. ϱ_7, ϱ_8 and ϱ_9 are the occupation probabilities of the levels 7, 8 and 9 within the S_0 band. The initial light intensities are $I_L(t', r, z = 0) = I_{0L} \exp(-t'^2/t_0^2 - r^2/r_0^2)$, $I_{ASE}(t', r, z = 0) = 0$, and $I_{REA}(t', r, z = 0) = 0$. $t_0 = \Delta t/[2(\ln 2)^{1/2}]$ is half the 1/e pulse width (Δt FWHM) and r_0 is the 1/e beam radius of the pump pulse (frequency ν_L). $N_{1'}$ and $N_{3'}$ are the ground-state and excited-state level populations, respectively, of the impurity molecules in the dye solution.

N_1 comprises the total population of the S_0 band. The first term in Equation 1 is responsible for two-photon absorption; $\sigma^{(2)}$ is the orientation-averaged two-photon-absorption cross-section. The

second term describes the stimulated emission. The third term takes amplified spontaneous emission into account. The fourth term gives the S_1–S_0 relaxation rate; $\tau_F = \eta_F \tau_{rad}$ is the fluorescence lifetime, where η_F is the fluorescence quantum efficiency and τ_{rad} is the radiative lifetime. The last term approximates the reabsorption of fluorescence light; σ_{REA} is the reabsorption cross-section.

Equation 2 contains two-photon absorption, S_{n1}–S_{n4} excited-state absorption, and S_{n1}–S_1 relaxation. Equation 3 is responsible for the S_1-state dynamics. The first term gives the level population by S_{n1}–S_1 relaxation. The second and third terms describe excited-state absorption at ν_L and ν_{ASE}, respectively. The next two terms depopulate level 3 by stimulated emission at ν_L and ν_{ASE}. The sixth term determines the reabsorption of fluorescence light. The last four terms describe relaxations.

Equations 4 to 6 handle level populations by excited-state absorption. Equation 7 considers fluorescence emission into the reabsorption region. The first term gives the filling of level 7. $e_{A,REA}$ is the fraction of fluorescence falling into the spectral reabsorption region. The second term describes the reabsorption of fluorescence, and the third term takes care of thermalization in the S_0 band. In Equation 8 the first term gives level population by stimulated emission while the second term takes care of thermalization. In Equation 9 the first term describes the fluorescence emission in the amplified spontaneous emission spectral region. $e_{T,ASE}$ presents the fraction of fluorescence falling into the transparent spectral region ($e_{T,ASE} + e_{A,REA} \approx 1$). The second term handles the amplified spontaneous emission, and the last term causes thermalization.

Equations 10 and 11 are included for the discussion of impurity effects. They describe the impurity bleaching in a three-level system with fast intermediate state (Fig. 1b) [28].

The change of pump-laser intensity is described by Equation 12. Two-photon absorption (first term), excited-state absorption (second and third terms), stimulated emission (fourth term), light scattering (fifth term) and impurity absorption (last term) are included. The generation of amplified spontaneous emission is described by Equation 13: the first term gives the seeding spontaneous emission in the transparent fluorescence region ($\pi r_0^2/l^2$ is the solid angle of efficient amplified spontaneous emission; l, sample length), the second term describes the stimulated amplification of the fluorescence, the third term takes care of excited-state absorption, and the last term considers scattering. Equation 14 describes the reabsorption of fluorescence along the light path: the first term gives the spontaneous emission, the second term is due to reabsorption and the last term takes care of scattering.

Because the S_n–S_1 relaxation times are short compared to the pulse durations, the steady-state solutions of Equations 2, 4, 5 and 6 are used leading to

$$N_2 = \frac{\tau_{23}\sigma^{(2)} I_L^2 N_1}{2(h\nu_L)^2 + \tau_{23}\sigma^{(2)} I_L^2 + h\nu_L \tau_{23}\sigma_{ex,24} I_L - h\nu_L \tau_{23}\sigma_{ex,24} I_L \Big/ \left(1 + \frac{h\nu_L}{\tau_{43}\sigma_{ex,24} I_L}\right)} \tag{15}$$

$$N_4 = \frac{N_2}{1 + \frac{h\nu_L}{\tau_{43}\sigma_{ex,24} I_L}} \tag{16}$$

$$N_5 = \frac{N_3}{1 + \frac{h\nu_L}{\tau_{53}\sigma_{ex,L} I_L}} \tag{17}$$

$$N_6 = \frac{N_3}{1 + \frac{h\nu}{\tau_{63}\sigma_{ex,ASE} I_{ASE}}} \tag{18}$$

The system of Equations 1, 3, 7 to 18 is solved numerically to analyse the S_0–S_n two-photon-

absorption dynamics. In the experiments the energy transmission

$$T_E = \int_0^\infty \left[\int_{-\infty}^{\infty} I_L(t', r, l)\,dt' \right] 2\pi r\,dr \Big/ \int_0^\infty \left[\int_{-\infty}^{\infty} I_L(t', r, 0)\,dt' \right] 2\pi r\,dr \qquad (19)$$

is measured as a function of input-pulse peak intensity I_{0L}. Temporal and spatial gaussian input-pulse shapes are assumed. A comparison of the experimental energy transmission curves with calculations allows one to determine the two-photon-absorption cross-section, $\sigma^{(2)}$, if the other dye parameters are known.

3. Dye parameters

The dyes rhodamine B dissolved in acidic methanol [29, 30] (0.003 mol dm^{-3} HCl added) and ethanol and rhodamine 6G dissolved in neutral methanol and ethanol are investigated (dyes from Kodak). A picosecond ruby laser is used for the two-photon absorption measurements. The dye parameters entering Equations 1 to 18 are summarized in Table I. The data are independent of the solvent methanol or ethanol within our experimental accuracy and, therefore, only a single set of data is listed. If dye parameters are varied in some calculations, the changes are explicitly stated. The origins of the data are specified in Table I. Most of the data of Table I are obtained from the absorption and emission spectra of Figs 2 to 4. The two-photon absorption cross-sections and some excited-state-absorption cross-sections are determined by the present analysis.

The absorption and emission spectra of rhodamine B and rhodamine 6G dissolved in methanol are presented in Figs 2 and 3, respectively. The corresponding absorption and emission spectra for the solvent ethanol are within the experimental accuracy identical to the methanolic solutions. Only

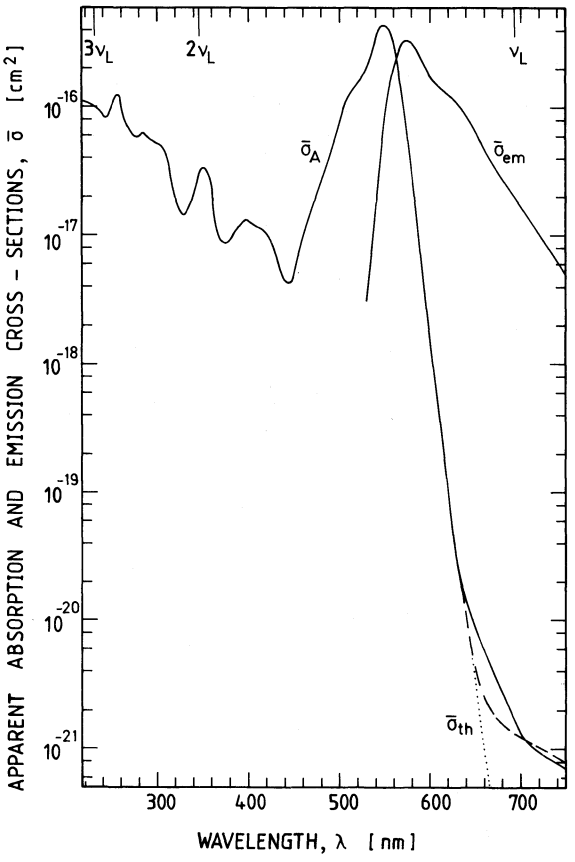

Figure 2 Absorption and emission spectra of rhodamine B in acidic methanol. $\bar{\sigma}_A$, apparent absorption cross-section. $\bar{\sigma}_{th}$, shape of absorption cross-section due to thermal level population. $\bar{\sigma}_{em}$, apparent emission cross-section. Absorption and emission spectrum of rhodamine B in ethanol is the same. The deviation in the long-wavelength absorption spectrum is indicated by the dashed curve.

TABLE I Dye Parameters

Parameter	Transition	Rhodamine B	Rhodamine 6G	Comments
Absorption cross-section				
$\sigma^{(2)}$ ($cm^4 s$)	S_0–S_{n1}	$(1.2 \pm 0.2) \times 10^{-48}$	$(1.8 \pm 0.2) \times 10^{-48}$	a
σ_{em} (cm^2)	$S_1 \rightarrow S_0$ (3 → 8)	$(1.9 \pm 0.2) \times 10^{-17}$	$(9 \pm 1) \times 10^{-18}$	b
σ_{ASE} (cm^2)	$S_1 \rightarrow S_0$ (3 → 9)	$(7 \pm 1.5) \times 10^{-17}$	$(7 \pm 1.5) \times 10^{-17}$	c
$\sigma_{ex,24}$ (cm^2)	$S_{n1} \rightarrow S_{n4}$ (2 → 4)	–	–	d
$\sigma_{ex,L}$ (cm^2)	S_1–S_{n2} (3 → 5)	$(1 \pm 0.3) \times 10^{-17}$	$(5 \pm 1) \times 10^{-18}$	e
$\sigma_{ex,ASE}$ (cm^2)	S_1–S_{n3} (3 → 6)	$(1 \pm 1) \times 10^{-17}$	$(1 \pm 1) \times 10^{-17}$	f
σ_{SCA} (cm^2)		2.1×10^{-22}	2.1×10^{-22}	g
σ_{IM} (cm^2)	(1′ → 2′)	2×10^{-17}	2×10^{-17}	h
Wavelengths				
λ_L (nm)		694.3	694.3	i
λ_{REA} (nm)	S_0–S_1 (7 → 3)	574	556	j
λ_{ASE} (nm)	S_1–S_0 (3 → 9)	646	626	j
Initial S_0-level population				
ϱ_1		1	1	k
ϱ_7		0.22	0.09	l
ϱ_8		6×10^{-8}	1.6×10^{-9}	l
ϱ_9		3×10^{-4}	2.1×10^{-4}	l
Fluorescence contributions				
$e_{T,ASE}$		0.125	0.25	j
$e_{A,REA}$		0.875	0.75	j
Relaxation rates				
τ_{23} (ps)	$S_{n1} \rightarrow S_1$ (2 → 3)	0.1	0.1	m
τ_{43} (ps)	$S_{n4} \rightarrow S_1$ (4 → 3)	0.1	0.1	m
τ_{53} (ps)	$S_{n2} \rightarrow S_1$ (5 → 3)	0.1	0.1	m
τ_{63} (ps)	$S_{n3} \rightarrow S_1$ (6 → 3)	0.1	0.1	m
τ_{rad} (ns)	$S_1 \rightarrow S_0$ (3 → 1)	4.7	4.7	n
τ_F (ps)	$S_1 \rightarrow S_0$ (3 → 1)	350	350	o
τ_v (ps)	$S_0(v) \rightarrow S_0(0)$	4	4	p
τ_{IM} (ps)	(3′ → 1′)	10	10	h
Two-photon saturation intensity				
$I_S^{(2)}$ ($W cm^{-2}$)		6.7×10^{10}	5.5×10^{10}	q

Concentration 0.04 mol dm^{-3}, solvent methanol. Data for solvent ethanol are identical, within experimental accuracy. Room temperature. Sample length 2 cm, beam radius $r_0 = 0.2$ mm.

[a] From Figs 6 and 7; this work
[b] From Figs 2 and 3; $\sigma_{em} = \bar{\sigma}_{em}(\lambda_L)$
[c] From Figs 2 and 3; $\sigma_{ASE} = \bar{\sigma}_{em}(\lambda_{ASE})$
[d] Not relevant because τ_{23} very short
[e] From Fig. 8; this work
[f] For rhodamine 6G [34, 35]; for rhodamine B assumed
[g] This work
[h] Assumed
[i] Ruby pump-laser frequency
[j] From Fig. 4
[k] Level 1 comprises whole S_0 band
[l] Calculated from $\varrho_i = N_i/N_0 = \bar{\sigma}_A(\lambda_i)/\bar{\sigma}_{em}(\lambda_i)$ (see Figs 2 and 3)
[m] Approximate values according to [39–42]
[n] For rhodamine B [43]; for rhodamine 6G [25, 33, 44, 45]
[o] For rhodamine 6G [25]; for rhodamine B, same value assumed
[p] Taken from [17]; see also [18]
[q] Equation 26 with $t_{eff} = \Delta t_L = 30$ ps

in the long-wavelength absorption wings of the S_0–S_1 transition are deviations observable, which are included in the figures (dashed curves for ethanol).

The apparent absorption cross-sections $\bar{\sigma}_A = -\ln(T/N_0 l)$ [21, 22] are obtained from transmission measurements with a spectrophotometer (T, transmission; N_0, total number density of dye molecules; l, sample length). Dye concentrations of 10^{-4} mol dm^{-3} and 0.04 mol dm^{-3} have been used in the absorption spectra measurements for $\bar{\sigma} > 2 \times 10^{-18}$ cm^2 and $\bar{\sigma} < 2 \times 10^{-18}$ cm^2, respectively.

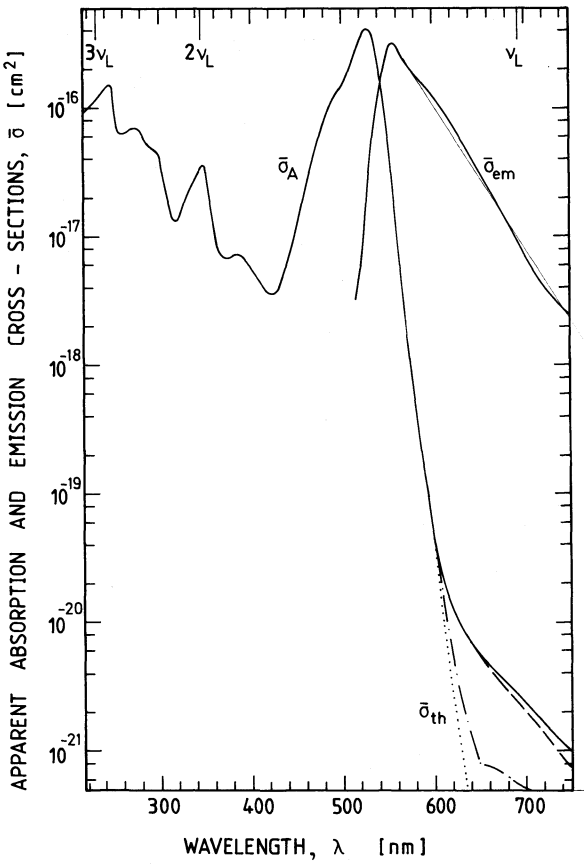

Figure 3 Absorption and emission spectra of rhodamine 6G in methanol. The meaning of the various curves is the same as in Fig. 2. Dash-dotted curve belongs to purified rhodamine 6G in methanol.

The apparent absorption cross-sections, $\bar{\sigma}(\nu)$, differ from the real absorption cross-sections $\sigma(\nu)$, which enter the system of Equations 1 to 18, by $\bar{\sigma}_A(\nu) = \alpha(\nu)/N_0$ and $\sigma_A(\nu) = \alpha(\nu)/N(\nu)$, where $\alpha(\nu)$ is the absorption coefficient (dimension cm^{-1}) and $N(\nu)$ is the number density of interacting molecules at frequency ν [21, 22]. For $\nu > \nu_{A,max}$ the apparent and real absorption cross-sections are thought to be approximately equal, i.e. $\bar{\sigma}_A(\nu) = \sigma_A(\nu)$ (all molecules take part in transitions; $\nu_{A,max}$ frequency of maximum S_0–S_1 absorption). For $\nu < \nu_{A,max}$ the real absorption cross-section $\sigma_A(\nu)$ is larger than the experimental absorption cross-section $\bar{\sigma}_A$, because $N(\nu) < N_0$ (only inhomogeneously broadened and thermally excited molecules take part in the S_0–S_1 absorption). The dotted curves in Figs 2 and 3 indicate the expected long-wavelength decay of the apparent absorption cross-sections due to thermal population of the states in the S_0 band ($\bar{\sigma}_{th}(\nu) = \bar{\sigma}_A(\nu_0) \exp[-h(\nu_0 - \nu)/kT]$ because $N_1(\nu) = N_1(\nu_0) \exp[-h(\nu_0 - \nu)/kT]$).

The residual absorption in the long-wavelength wings of Figs 2 and 3 above the dotted curves is thought to be mainly due to impurity absorption. The rhodamine-6G–methanol solution was purified by recrystallization from methanol, resulting in a remarkable drop of the long-wavelength-absorption edge (dash-dotted curve in Fig. 3).

Transmission loss by light scattering was analysed by measuring the scattered laser light perpendicular to the direction of laser propagation and comparing the signal with the scattered light in a diluted milk solution. The expected transmission due to scattering was found to be $T_{SCA} \simeq 0.99$ for all solutions investigated (0.04 M rhodamine 6G and rhodamine B in 2-cm-long cells).

The S_0–T singlet–triplet absorption is estimated from the phosphorescence lifetime τ_{ph} to be negligibly small ($\sigma_{T,max} \approx \bar{\sigma}(\nu_{A,max})\tau_{ph}/\tau_{rad} \approx 10^{-24} cm^2$ [23]).

The apparent stimulated-emission-cross-section curves of Figs 2 and 3 are calculated from our

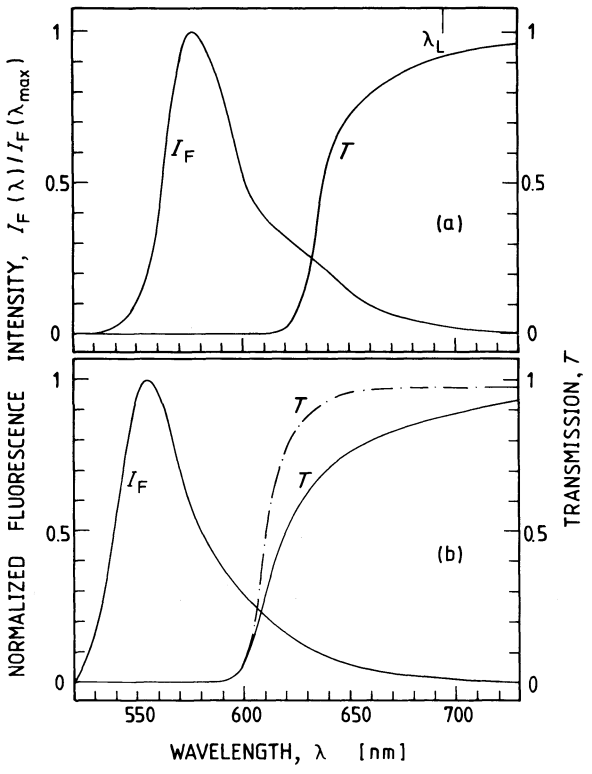

Figure 4 Fluorescence spectra of (a) rhodamine B in acidic methanol and (b) rhodamine 6G in methanol. The transmission curves belong to 0.04 M dye solutions in 2-cm-long samples. Dash-dotted curve is obtained for purified rhodamine 6G in methanol.

measured fluorescence spectra (excitation source is a spectrally filtered tungsten lamp; backward fluorescence is detected with a spectrograph and Tracor DARRS diode array system) by use of the relation [16, 22, 31]

$$\bar{\sigma}_{em}(\lambda) = \lambda^4 \frac{\eta_F}{\eta_A} \frac{I_F(\lambda)}{\int_{em} I_F(\lambda)\,d\lambda} \frac{\int_{em} I_F(\lambda)\lambda\,d\lambda}{\int_{em} I_F(\lambda)\lambda^4\,d\lambda} \int_{abs} \frac{\bar{\sigma}_A(\lambda)}{\lambda}\,d\lambda \tag{20}$$

$I_F(\lambda)$ is the detected fluorescence signal (photons per wavelength unit) at wavelength λ. The fluorescence integration ranges over the S_1–S_0 fluorescence band. The absorption integral spans over the S_0–S_1 absorption band. η_F and η_A are the mean refractive indices of the dye solutions in the fluorescence and absorption region, respectively. The determined stimulated-emission-cross-section curves are in good agreement with reported spectra (rhodamine B in methanol [32], rhodamine B in ethanol [33], rhodamine 6G in methanol [33], rhodamine 6G in ethanol [32]). In the long-wavelength region, $\nu < \nu_{em,max}$, the apparent and real stimulated-emission cross-sections are thought to be equal and identical to the real absorption cross-sections [$\bar{\sigma}_{em}(\nu) = \sigma_{em}(\nu) = \sigma_A(\nu)$ for $\nu < \nu_{em,max}$] [21, 22].

Fig. 4 depicts the fluorescence spectra of rhodamine B and rhodamine 6G together with the transmission of light through a cell of length $l = 2$ cm. The dash-dotted curve in Fig. 4b belongs to the purified rhodamine-6G–methanol solution. The steep rise of transmission determines the wavelength of amplified spontaneous emission λ_{ASE} and the fluorescence contribution $e_{T,ASE}$ to the amplified spontaneous emission. The region of low transmission locates the fluorescence reabsorption (centre wavelength λ_{REA}) and the fluorescence contribution $e_{A,REA}$ to reabsorption.

The excited-state absorption $\sigma_{ex,ASE}$ for rhodamine 6G is extracted from gain measurements of [34, 35] where $\sigma_{em,ASE} - \sigma_{ex,ASE}$ is measured and from the fluorescence spectrum of Fig. 3 ($\sigma_{em,ASE}$). For

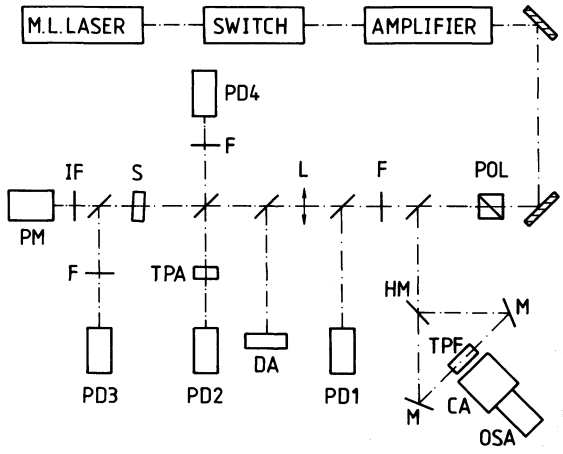

Figure 5 Experimental arrangement: POL, linear-polarizer; F, filters; PD1–PD4, photodetectors; HM, 50% mirror; M, mirrors; TPF, two-photon fluorescence cell; CA, camera; OSA vidicon of optical spectrum analyser; DA, diode array; TPA, CdS crystal for intensity detection; L, lens; S, sample; IF, interference filter; PM, photomultiplier.

rhodamine B an explicit value of $\sigma_{ex,ASE}$ is not available, but from the laser action of rhodamine B at ν_{ASE} in dye lasers it is known that $\sigma_{ex,ASE} \ll \sigma_{em,ASE}$.

4. Experiments

In the experiments the two-photon-absorption cross-sections, $\sigma^{(2)}$, and the excited-state-absorption cross-sections, $\sigma_{ex,L}$, were determined. The other dye parameters influencing the pulse propagation through the dyes have been described in the previous section. The intensity-dependent energy transmission of single picosecond ruby laser pulses through 0.04 M methanolic and ethanolic solutions of rhodamine B and rhodamine 6G was measured (sample length $l = 2$ cm). The transmission behaviour depends on $\sigma^{(2)}$ and $\sigma_{ex,L}$. The transmission measurement of a delayed probe pulse at frequency ν_L allows the determination of $\sigma_{ex,L}$ [36].

The experimental arrangement is shown in Fig. 5. A passively mode-locked ruby laser generates a train of picosecond pulses. A krytron-triggered Pockels-cell shutter selects single picosecond pulses from the generated pulse trains. A ruby laser amplifier increases the energy of the selected pulses. A two-photon fluorescence arrangement is used for pulse-duration measurements [8]. Rhodamine 6G in ethanol (2.5×10^{-3} M) is used as a two-photon fluorescence dye. The beam profile is monitored with a diode array DA.

The energy transmission through the investigated dyes in sample S is detected with the photocells PD1 and PD3. The peak intensity of the light pulses is determined by two-photon-transmission measurements through a CdS crystal [37] with detectors PD1 and PD2.

For the determination of the S_1–S_2 excited-state-absorption cross-section, $\sigma_{ex,L}$, a glass plate is inserted behind the sample S in order to reflect a small portion of the laser light back through the sample. The transmission of the backward probe pulse is measured with detectors PD3 and PD4 [36]. The amplification or attenuation of the backward probe pulse depends on the S_1-state population (determined by $\sigma^{(2)}$) and the effective cross-section $\sigma_{em} - \sigma_{ex,L}$ ($\sigma_{em} > \sigma_{ex,L}$, amplification; $\sigma_{em} < \sigma_{ex,L}$, attenuation).

Additionally, the forward fluorescence and amplified spontaneous emission is monitored with photomultiplier PM. Insertion of a broad-band interference filter IF allows the registration of the spectrally integrated fluorescence light. With a monochromator instead of the interference filter, the spectrally resolved fluorescence emission is detected. The fluorescence signal at high intensities depends on the effective emission cross-section, $\sigma_{ASE} - \sigma_{ex,ASE}$, and the S_1-state level population, which is determined by $\sigma^{(2)}$ and $\sigma_{em} - \sigma_{ex,L}$ (see below).

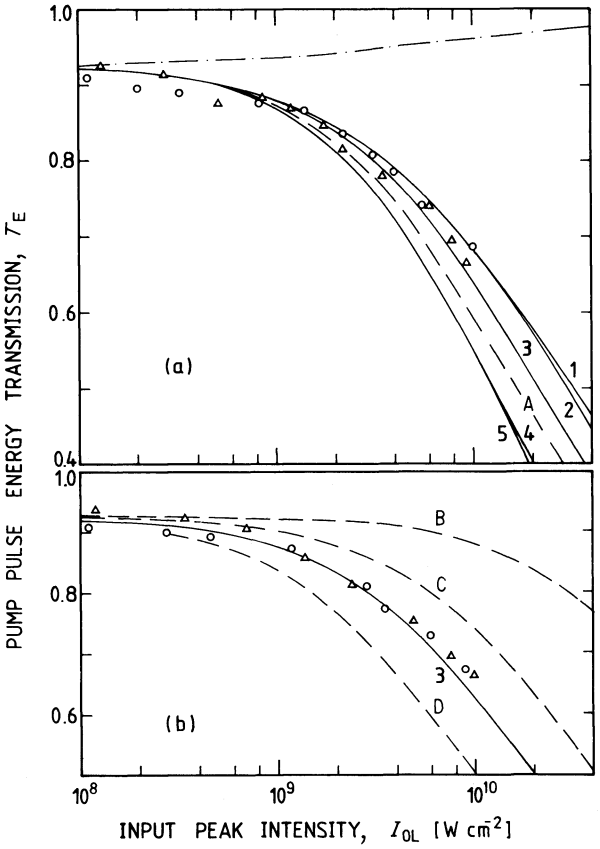

Figure 6 Energy transmission of ruby laser pump pulses through rhodamine-B solutions. Sample length 2 cm. Concentration 0.04 mol dm^{-3}. Solvents are acidic methanol (○) and untreated ethanol (△). (a) Pulse duration $\Delta t = 30$ ps (FWHM); (b) $\Delta t = 15$ ps. The curves are calculated with the data of Table I except as follows. Solid curves: (1) $\sigma_{ASE} = \sigma_{ex,ASE} = \sigma_{ex,L} = 0$, $\sigma_{em} = 10^{-17}$ cm^2; (2) $\sigma_{ex,ASE} = \sigma_{ex,L} = 0$, $\sigma_{em} = 10^{-17}$ cm^2, $\sigma_{ASE} = 6 \times 10^{-17}$ cm^2; (3) no changes (best-fit curve); (4) $\sigma_{em} = \sigma_{ex,ASE} = 0$, $\sigma_{ex,L} = 3.5 \times 10^{-18}$ cm^2, $\sigma_{ASE} = 10^{-16}$ cm^2, $\tau_v = 1$ ps; (5) $\sigma_{em} = \sigma_{ASE} = \sigma_{ex,ASE} = 0$, $\sigma_{ex,L} = 3.5 \times 10^{-18}$ cm^2. Dashed curves: (A) $\sigma^{(2)} = 1.2 \times 10^{-48}$ cm^4 s, $\sigma_{em} = \sigma_{ASE} = \sigma_{ex,L} = \sigma_{ex,ASE} = 0$, $\tau_{IM} = 0$; (B) $\sigma^{(2)} = 1 \times 10^{-49}$ cm^4 s, $\sigma_{em} = \sigma_{ASE} = \sigma_{ex,L} = \sigma_{ex,ASE} = 0$, $\tau_{IM} = 0$; (C) $\sigma^{(2)} = 5 \times 10^{-49}$ cm^4 s, $\sigma_{em} = \sigma_{ASE} = \sigma_{ex,L} = \sigma_{ex,ASE} = 0$, $\tau_{IM} = 0$; (D) $\sigma^{(2)} = 2 \times 10^{-48}$ cm^4 s, $\sigma_{em} = \sigma_{ASE} = \sigma_{ex,L} = \sigma_{ex,ASE} = 0$, $\tau_{IM} = 0$. Dash-dotted curve: $\sigma^{(2)} = 0$ (bleaching of impurities).

5. Results

The experimental results are shown by data points in Figs 6 to 9. The forward energy transmissions of the intense ruby laser pulses are shown in Figs 6 and 7 for rhodamine B and rhodamine 6G, respectively. The curves in Figs 6a and 7a are for $\Delta t_L = 30$ ps and those in Figs 6b and 7b for $\Delta t_L = 15$ ps. The 15 ps ruby laser pulses were obtained by passing the pulses through a saturable absorber after the amplifier (absorber DDI in methanol, transmission $T_0 = 10^{-4}$) [38]. The energy transmission is independent of the pulse duration within the experimental accuracy. The closed circles in Fig. 7a depict the two-photon transmission of the purified rhodamine-6G–methanol solution. At high intensities the energy transmissions of the purified solution approach the energy transmission of the untreated solution, indicating the bleaching of the impurity absorption at high intensities. The solid curves in Figs 6 and 7 are calculated with the aid of Equations 1 to 19 using the parameters listed in the figure captions and in Table I (for discussion of curves, see below). The best fits of the calculations to the data points give the two-photon-absorption cross-sections of $\sigma^{(2)} = (1.2 \pm 0.2) \times 10^{-48}$ cm^4 s for rhodamine B and $(1.8 \pm 0.2) \times 10^{-48}$ cm^4 s for rhodamine 6G. Our results agree reasonably well with previously reported values of $(1.48 \pm 0.7) \times 10^{-48}$ cm^4 s for rhodamine B and $(3.55 \pm 1.7) \times 10^{-48}$ cm^4 s for rhodamine 6G [3].

The backward energy transmission of a reflected weak probe pulse (frequency ν_L, distance between end of sample and reflection glass plate 1.2 cm, reflection factor 0.04) as a function of input pump-pulse intensity (duration $\Delta t_L = 30$ ps) is shown in Fig. 8a for rhodamine B in methanol and in Fig. 8b for rhodamine 6G in methanol. At low input intensity the backward transmission is equal to the small signal forward transmission (ground-state absorption, no S_1-state population). With

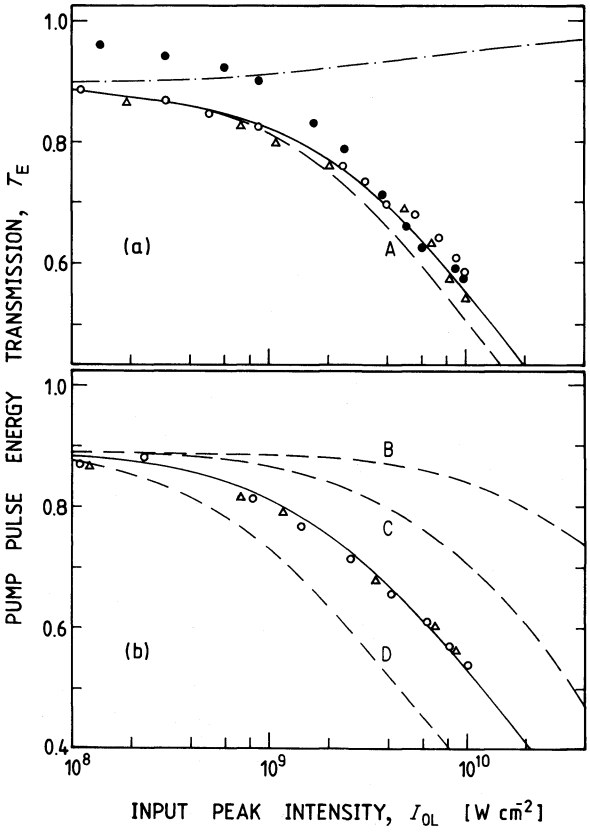

Figure 7 Energy transmission of ruby laser pump pulses through rhodamine-6G solutions. Sample length 2 cm. Concentration 0.04 mol dm^{-3}. Solvents are methanol (○) and ethanol (△). Closed circles belong to purified rhodamine 6G in ethanol. (a) Pulse duration Δt = 30 ps; (b) Δt = 15 ps. Solid curves give best-fit (data of Table I). Dash-dotted curve, $\sigma^{(2)} = 0$ (bleaching of impurities). Dashed curves, data of Table I except as follows: (A) $\sigma_{em} = \sigma_{ASE} = \sigma_{ex,ASE} = \sigma_{ex,L} = 0$, $\tau_{IM} = 0$; (B) $\sigma^{(2)} = 1 \times 10^{-49}$ cm^4 s, $\sigma_{em} = \sigma_{ASE} = \sigma_{ex,ASE} = \sigma_{ex,L} = 0$, $\tau_{IM} = 0$; (C) $\sigma^{(2)} = 5 \times 10^{-49}$ cm^4 s, $\sigma_{em} = \sigma_{ASE} = \sigma_{ex,ASE} = \sigma_{ex,L} = 0$, $\tau_{IM} = 0$; (D) $\sigma^{(2)} = 4 \times 10^{-48}$ cm^4 s, $\sigma_{em} = \sigma_{ASE} = \sigma_{ex,ASE} = \sigma_{ex,L} = 0$, $\tau_{IM} = 0$.

increasing input intensity the backward transmission slightly rises. For the purified rhodamine-6G–methanol solution the backward transmission rises above 1 (amplification). This fact indicates that the excited-state-absorption cross-section, $\sigma_{ex,L}$, is less than the stimulated-emission cross-section. The rise of transmission is similar for untreated and purified solution. This behaviour indicates a fast absorption recovery time of the impurity molecules (bleached impurity molecules return to the ground state within the delay time of the probe pulse). An absorption recovery time of τ_{IM} = 10 ps is assumed in the calculation. The backward probe pulse transmission curves of Fig. 8 are calculated by use of the transmission formula $T_B = \exp\{-\sigma_{ex,L}\int_0^l N_3(z)\,dz + \sigma_{em}\int_0^l [N_3(z) - N_8(z)]\,dz\}$ [36]. N_3 and N_8 are determined by solution of the system of Equations 1 to 18 with the data of Table I. In Fig. 8a (rhodamine B), curve 1 represents the best-fit ($\sigma_{ex,L} = 1 \times 10^{-17}$ cm^2, $\sigma_{em} = 1.9 \times 10^{-17}$ cm^2), curve 2 belongs to $\sigma_{ex,L} = \sigma_{em} = 1.9 \times 10^{-17}$ cm^2. In Fig. 8b (rhodamine 6G), the best-fit T_B curve 2 ($\sigma_{ex,L} = 5 \times 10^{-18}$ cm^2, $\sigma_{em} = 9 \times 10^{-18}$ cm^2) and the curves for $\sigma_{ex,L} = 0$, $\sigma_{em} = 9 \times 10^{-18}$ cm^2 (curve 1) and $\sigma_{ex,L} = \sigma_{em} = 9 \times 10^{-18}$ cm^2 (curve 3) are shown. The dash-dotted curve belongs to purified rhodamine 6G in methanol (same parameters as curve 2).

The intensity dependence of the forward spontaneous emission and amplified spontaneous emission is shown in Fig. 9a and b for rhodamine B and rhodamine 6G, respectively (Δt_L = 30 ps). The experimental data give no indication of an increase of fluorescence by amplified spontaneous emission. The fluorescence signals are only measured in arbitrary units and they are adjusted to the theoretical curves of Fig. 9 in the intensity region $I_{0L} < 10^9$ W cm^{-2}.

The influence of σ_{em} and $\sigma_{ex,L}$ on amplification of spontaneous emission is illustrated in Fig. 9a. An increase of σ_{em} or an increase of $\sigma_{ex,L}$ reduces the effect of amplified spontaneous emission,

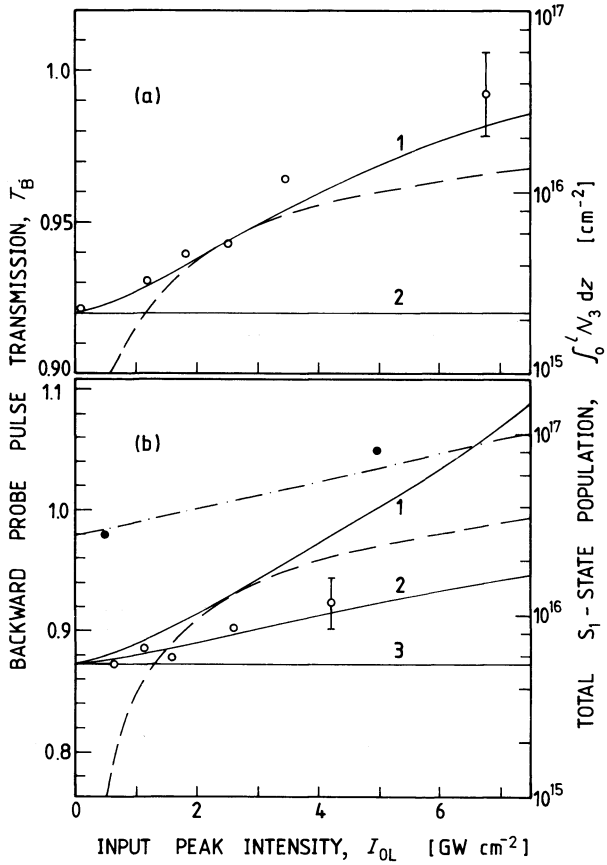

Figure 8 Energy transmission of weak ruby laser probe pulse retro-reflected through the dye sample from a glass plate at a distance of 1.2 cm behind the end of the sample cell. The dashed curves indicate the length-integrated S_1-state populations generated by the pump pulse. (a) Rhodamine B in acidic methanol. Solid curve 1, best-fit to experimental data ($\sigma_{ex,L} = 10^{-17}\,cm^2$, $\sigma_{em} = 1.9 \times 10^{-17}\,cm^2$, see Table I); curve 2, $\sigma_{ex,L} = \sigma_{em} = 1.9 \times 10^{-17}\,cm^2$. (b) Rhodamine 6G in ethanol. Solid curves belong to parameters of Table I except as follows: (1) $\sigma_{ex,L} = 0$, $\sigma_{em} = 9 \times 10^{-18}\,cm^2$; (2) best-fit to experimental data ($\sigma_{ex,L} = 5 \times 10^{-18}\,cm^2$, $\sigma_{em} = 9 \times 10^{-18}\,cm^2$); (3) $\sigma_{ex,L} = \sigma_{em} = 9 \times 10^{-18}\,cm^2$. Dash-dotted curve belongs to purified solution (same parameters as curve 2).

because σ_{em} as well as $\sigma_{ex,L}$ reduces the S_1-state population. The suppression of amplified spontaneous emission is more pronounced for shorter relaxation times τ_v in the S_0-band (dashed curve compared with curve 3) because fast depopulation of level 8 reduces the S_1-state population (reduction of bottleneck effect, see below). In Table I, $\tau_v = 4$ ps is listed [17]. Relaxation from the high-lying level 8 may be considerably faster than 4 ps, which represents the recovery time of the ground-state absorption [17].

The influence of $\sigma_{ASE} - \sigma_{ex,ASE}$ on amplified spontaneous emission is studied in Fig. 9b. Large $\sigma_{ASE} - \sigma_{ex,ASE}$ values (curve 1, $\tau_v = 4$ ps) result in a strong increase of the forward fluorescence signal as soon as $N_3 > N_9$. For $\sigma_{ASE} = \sigma_{ex,ASE}$ (curve 3), amplified spontaneous emission and excited-state absorption compensate each other and the forward fluorescence emission is approximately equal to the forward spontaneous emission (slight difference because $N_6 \neq N_9$). For $\sigma_{ex,ASE} > \sigma_{ASE}$ (curve 4) the forward signal falls below the spontaneous fluorescence signal because of absorption of spontaneous emission along the light path.

The dynamics of the S_0–S_n two-photon absorption is illustrated by theoretical calculations. In Figs 6 and 7, energy transmission curves are calculated for various parameters of the two-photon-absorption cross-section, $\sigma^{(2)}$ (dashed curves, $\sigma_{em} = \sigma_{ex,L} = \sigma_{ASE} = \sigma_{ex,ASE} = 0$, $\tau_{IM} = 0$) and single-photon cross-sections σ_{em}, σ_{ASE}, $\sigma_{ex,L}$ and $\sigma_{ex,ASE}$ (solid curves). The dashed curves in Figs 6b and 7b show the decrease in energy transmission with increasing $\sigma^{(2)}$ value. The solid curves in Fig. 6a illustrate the influence of the single-photon cross-sections: dominant stimulated emission $\sigma_{em} > \sigma_{ex,L}$ raises the energy transmission (curve 1 compared to dashed curve, $\sigma_{em} = 10^{-17}\,cm^2$, $\sigma_{ex,L} = \sigma_{ASE} = \sigma_{ex,ASE} = 0$). The effect is more pronounced for longer pulse durations (no curve

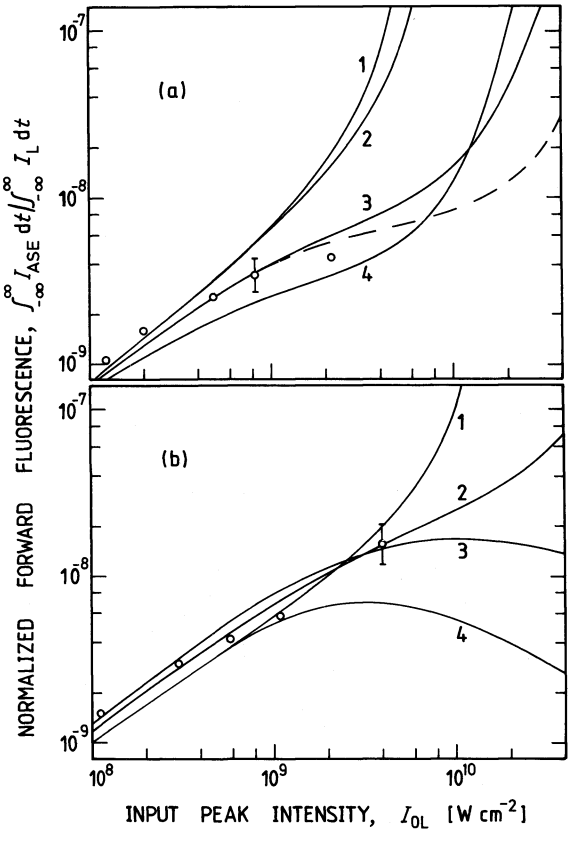

Figure 9 Forward fluorescence emission as a function of input peak pulse intensity. The experimental points are adjusted to the curves in the intensity region $I_{0L} < 10^9\,W\,cm^{-2}$. (a) Rhodamine B in acidic methanol. Influence of σ_{em} and $\sigma_{ex,L}$ on amplified spontaneous emission is studied. Curves belong to data of Table I ($\sigma_{ASE} = 7 \times 10^{-17}\,cm^2$, $\sigma_{ex,ASE} = 10^{-17}\,cm^2$) except: (1) $\sigma_{em} = \sigma_{ex,L} = 0$; (2) $\sigma_{em} = 0$, $\sigma_{ex,L} = 10^{-17}\,cm^2$; (3) $\sigma_{em} = 1.9 \times 10^{-17}\,cm^2$, $\sigma_{ex,L} = 10^{-17}\,cm^2$; (4) $\sigma_{em} = 5 \times 10^{-17}\,cm^2$, $\sigma_{ex,L} = 0$. Dashed curve, as solid curve 3 except $\tau_v = 1$ ps (experimental). (b) Rhodamine 6G in methanol. Influence of σ_{ASE} and $\sigma_{ex,ASE}$ on amplified spontaneous emission is studied. Curves belong to data of Table I ($\sigma_{em} = 9 \times 10^{-18}\,cm^2$, $\sigma_{ex,L} = 5 \times 10^{-18}\,cm^2$, $\tau_v = 4$ ps) except: (1) $\sigma_{ASE} = 7 \times 10^{-17}\,cm^2$, $\sigma_{ex,ASE} = 1 \times 10^{-17}\,cm^2$ (experimental); (2) $\sigma_{ASE} = 3 \times 10^{-17}\,cm^2$, $\sigma_{ex,ASE} = 10^{-17}\,cm^2$; (3) $\sigma_{ASE} = \sigma_{ex,ASE} = 10^{-17}\,cm^2$; (4) $\sigma_{ASE} = 7 \times 10^{-17}\,cm^2$, $\sigma_{ex,ASE} = 1.3 \times 10^{-16}\,cm^2$.

shown). Additional amplified spontaneous emission $\sigma_{ASE} - \sigma_{ex,ASE} > 0$ reduces the effect of stimulated emission at high intensities due to depopulation of the S_1 state (curve 2, $\sigma_{em} = 10^{-17}\,cm^2$, $\sigma_{ex,L} = 0$, $\sigma_{ASE} = 6 \times 10^{-17}\,cm^2$, $\sigma_{ex,ASE} = 0$). Dominant excited-state absorption $\sigma_{ex,L} > \sigma_{em}$ lowers the energy transmission (curve 5 compared to dashed curve, $\sigma_{em} = 0$, $\sigma_{ex,L} = 3.5 \times 10^{-18}\,cm^2$, $\sigma_{ASE} = \sigma_{ex,ASE} = 0$). The reduction of transmission increases with pulse duration (no curve shown). Additional amplified spontaneous emission reduces the effect of excited-state absorption at high intensities because amplified spontaneous emission depopulates the S_1-state (curve 4, $\sigma_{em} = 0$, $\sigma_{ex,L} = 3.5 \times 10^{-18}\,cm^2$, $\sigma_{ASE} = 6 \times 10^{-17}\,cm^2$, $\sigma_{ex,ASE} = 0$). Curve 3 represents the best fit to experimental data. The transmission is slightly higher than calculated by neglecting the single-photon effects in the S_1 state.

The intensity-dependent level populations at the middle of the pump pulse (time position $t = 0$ ps; pulse duration $\Delta t = 30$ ps) are illustrated in Figs 10 to 15.

In Fig. 10 the situation $\sigma_{em} = \sigma_{ex,L} = 0$ is considered. At the cell entrance (solid curves) the ground-state population is somewhat depleted at high pump intensities. The population accumulates in the S_1 state. Amplified spontaneous emission has no influence. Towards the end of the cell (dashed curves) the pump pulse is attenuated and no ground-state depletion is observed. In the case of dominant amplified spontaneous emission ($\sigma_{ASE} > \sigma_{ex,ASE}$, long-dashed curves) the S_1-state population is limited by amplified spontaneous emission. This effect is reduced by populating the terminal level 9 of the amplified spontaneous-emission transition (bottle-neck due to finite thermalization time τ_v). The short-dashed curves belong to $\sigma_{ASE} \leqslant \sigma_{ex,ASE}$. If there is no difference between $\sigma_{ASE} \leqslant \sigma_{ex,ASE}$ and $\sigma_{ASE} > \sigma_{ex,ASE}$, then only the long-dashed curves are shown.

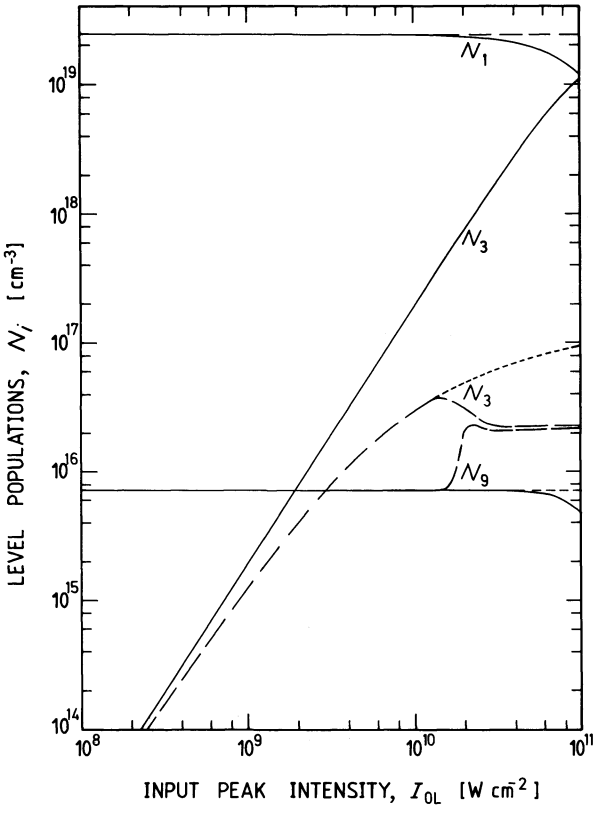

Figure 10 Level population as a function of input pulse peak intensity at cell entrance (solid curves) and cell exit (dashed curves). Data are for rhodamine B in acidic methanol (Table I) except $\sigma_{em} = \sigma_{ex,L} = 0$. Time position $t = 0$ (middle of pump pulse). Pulse duration $\Delta t = 30$ ps. At cell entrance, curves are independent of σ_{ASE} and $\sigma_{ex,ASE}$. At cell exit, long-dashed curves are for $\sigma_{ASE} = 6 \times 10^{-17}$ cm^2 and $\sigma_{ex,ASE} = 0$. The short-dashed curves are for $\sigma_{ASE} - \sigma_{ex,ASE} \leqslant 0$.

The case of $\sigma_{em} = 0$ and $\sigma_{ex,L} > 0$ is illustrated in Fig. 11. The S_1-state level population N_3 is reduced compared to the previous case because the excited-state absorption absorbs pump-laser photons without elevating molecules from the ground state. The ground-state depletion at high pump intensities is reduced. The effect of amplified spontaneous emission towards the end of the dye cell is reduced because of the weaker S_1-state population (long-dashed curves).

The situation of $\sigma_{em} = \sigma_{ex,L} = 10^{-17}$ cm^2 is studied in Fig. 12. The stimulated emission populates the terminal level 8 in the S_0 state. At high intensities N_8 approaches N_3 (bottleneck effect due to finite τ_v value; $\tau_v = 4$ ps used). The S_1-state level population is reduced because the S_1 level populates the terminal level 8 in the S_0 band. The ground-state depletion (N_1 comprises N_7, N_8, N_9) is reduced. Towards the end of the cell the pump pulse is attenuated and the S_1-state population is too low for an observable amplified spontaneous emission effect (curves with $\sigma_{ASE} > \sigma_{ex,ASE}$ and $\sigma_{ASE} \leqslant \sigma_{ex,ASE}$ are identical).

The level populations in the case of $\sigma_{em} > 0$ and $\sigma_{ex,L} = 0$ are shown in Fig. 13. The terminal level 8 is populated as in the case of $\sigma_{em} = \sigma_{ex,L} \neq 0$. The S_1-state population reaches slightly higher values because no excited-state-absorption loss is present. The ground-state depletion is small. The pump pulse is less strongly attenuated in its pass through the sample (see curve 1 in Fig. 6a). At high pump intensities amplified spontaneous emission builds up in the case of $\sigma_{ASE} - \sigma_{ex,ASE} > 0$ (long-dashed curves) and limits the S_1-state population towards the end of the sample (bottleneck effect for terminal level 9). The short-dashed curves belong to $\sigma_{ASE} - \sigma_{ex,ASE} \leqslant 0$.

The influence of the thermalization time τ_v on the level populations is illustrated in Fig. 14. The populations in the middle of the cell are shown ($z = 1$ cm). The solid curves belong to $\tau_v = 4$ ps and the dashed curves to $\tau_v = 1$ ps. The influence on amplified spontaneous emission is shown in Fig.

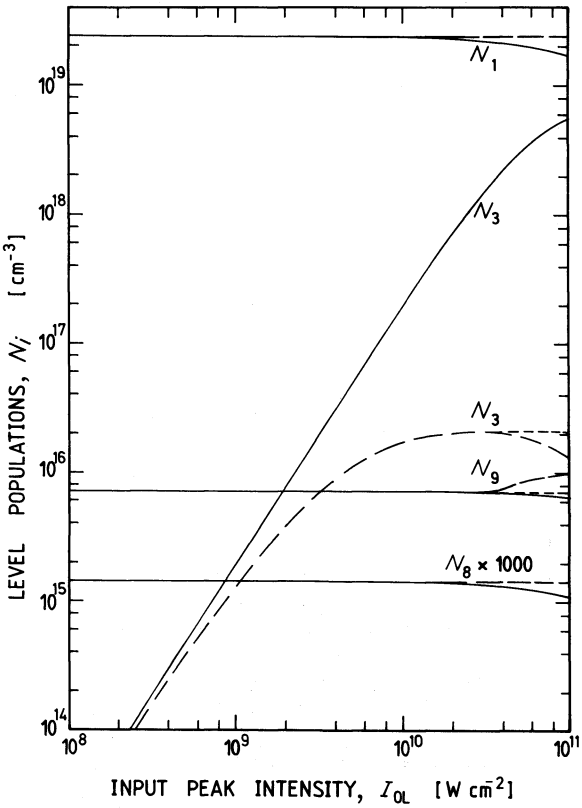

Figure 11 Level populations as a function of input pulse peak intensity at cell entrance (solid curves) and cell exit (dashed curves). Data are for rhodamine B in acidic methanol (Table I) except $\sigma_{em} = 0$, $\sigma_{ex,L} = 10^{-17}$ cm^2. Time position $t = 0$, $\Delta t = 30$ ps. Curves as in Fig. 10.

14a and the influence of stimulated emission is depicted in Fig. 14b. The bottleneck effect is shifted to higher pump intensities for shorter τ_v values.

The level populations for the experimental situation of rhodamine 6G in methanol are plotted in Fig. 15 (best-fit parameters used; time $t = 0$, pulse duration $\Delta t = 30$ ps). The ground-state depopulation is negligibly small over the experimental intensity region. Amplified spontaneous emission does not occur.

The influence of the two-photon absorption dynamics on the temporal pulse shape is analysed in Fig. 16. The pulse shapes $I_L(t', r = 0, l)/I_L(t, r = 0, z = 0)$ are shown. In Fig. 16a pulse deformation in the rhodamine-6G sample is shown for various input pulse intensities (best-fit parameters used in calculations). With increasing input pulse intensity the transmitted pulses are broadened. In Fig. 16b the influence of various dye parameters on the output pulse shape is analysed ($I_{0L} = 4 \times 10^{-10}$ W cm^{-2}). Seven different situations are considered:

(i) In the case of $\sigma_{em} = \sigma_{ex,L} = 0$ (no stimulated emission) and $\sigma_{ASE} - \sigma_{ex,ASE} \leqslant 0$ (no amplified spontaneous emission) only two-photon absorption occurs (curve 3). Pulse broadening due to two-photon absorption is observed. The ground-state depopulation at very high intensities causes a slightly asymmetric pulse formation due to reduced losses towards the end of the pulse.

(ii) The situation of $\sigma_{em} = \sigma_{ex,L} = 10^{-17}$ cm^2 and $\sigma_{ASE} - \sigma_{ex,ASE} \leqslant 0$ is shown by curve 4. The shape is similar to case (i) only the transmission is slightly lower because of excited-state absorption.

(iii) For $\sigma_{em} - \sigma_{ex,L} < 0$ (dominant excited-state absorption) and $\sigma_{ASE} - \sigma_{ex,ASE} \leqslant 0$ (no amplified spontaneous emission) the absorption in the trailing part of the pulse is enhanced. The pulse broadening due to two-photon absorption is reduced (curve 5).

(iv) In the case of dominant excited-state absorption at ν_L and additional amplified spontaneous

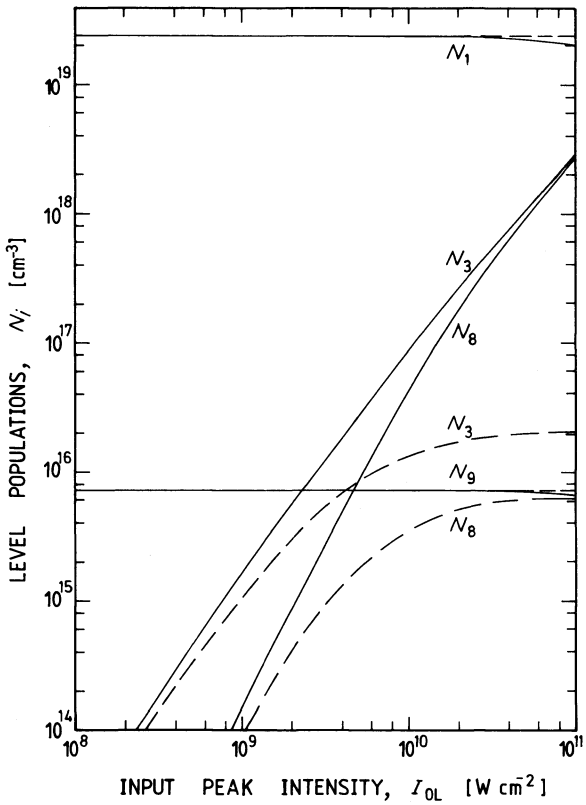

Figure 12 Level populations at cell entrance (solid curves) and cell exit (dashed curves). Data are for rhodamine B in methanol (Table I) except $\sigma_{em} = \sigma_{ex,L} = 10^{-17}$ cm^2. Time position $t = 0$, $\Delta t = 30$ ps. Curves as in Fig. 10 (short-dashed curves are not shown because they are identical to the long-dashed curves).

emission at $\nu_{ASE}(\sigma_{em} - \sigma_{ex,L} < 0$ and $\sigma_{ASE} - \sigma_{ex,ASE} > 0)$ both effects enhance the absorption in the trailing part of the pulse and slight pulse shortening may be achieved (curve 6).

(v) If $\sigma_{em} - \sigma_{ex,L} = 0$ (no stimulated emission) and $\sigma_{ASE} - \sigma_{ex,ASE} > 0$ (amplified spontaneous emission) ground-state depopulation is hindered. The two-photon absorption broadens the pulse shape (as in curve 4).

(vi) Dominant stimulated emission ($\sigma_{em} - \sigma_{ex,L} > 0$) reduces the two-photon absorption losses. At high pump intensities the stimulated emission saturates around the pulse maximum because of filling of level 8 (Fig. 15b). In the trailing part the pulse is amplified as the population of level 8 decays (for $\tau_v \to 0$ no amplification occurs, i.e. $I_{out}(t)/I_{in}(t) \leqslant 1$ for all t). The situation is illustrated by curve 1 where no amplified spontaneous emission is present ($\sigma_{ASE} - \sigma_{ex,ASE} \leqslant 0$).

(vii) In the case of simultaneous stimulated emission at $\nu_L(\sigma_{em} - \sigma_{ex,L} > 0)$ and amplified spontaneous emission at $\nu_{ASE}(\sigma_{ASE} - \sigma_{ex,ASE} > 0)$ both processes deform the pulse shape (curve 2). The amplification in the trailing part of the pulse is reduced by the amplified spontaneous emission (reduction of S_1-state population).

6. Analytical estimates

Concentrating on two-photon absorption and non-bleachable single-photon absorption Equation 12 simplifies to

$$\frac{\partial I_L}{\partial z} = -\alpha I_L - \sigma^{(2)} \frac{N_0}{h\nu_L} I_L^2 \tag{21}$$

Here ground-state depopulation is neglected. The absorption coefficient $\alpha = -\ln(T)/l$ takes care of the small-signal absorption of the sample (contributions from impurities and scattering

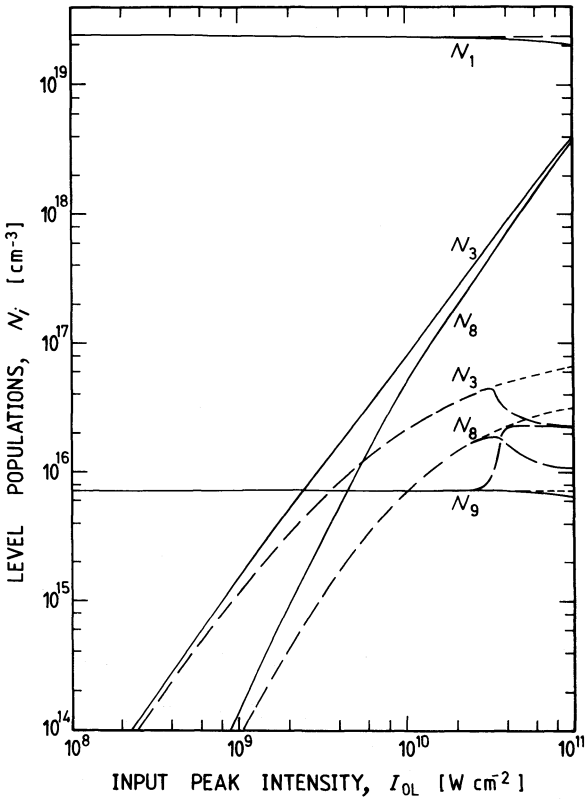

Figure 13 Level populations at cell entrance (solid curves) and cell exit (dashed curves). Data are for rhodamine B in methanol (Table I) except $\sigma_{em} = 10^{-17}\,cm^2$ and $\sigma_{ex,L} = 0$. Time position $t = 0$, $\Delta t = 30\,ps$. Curves as in Fig. 10.

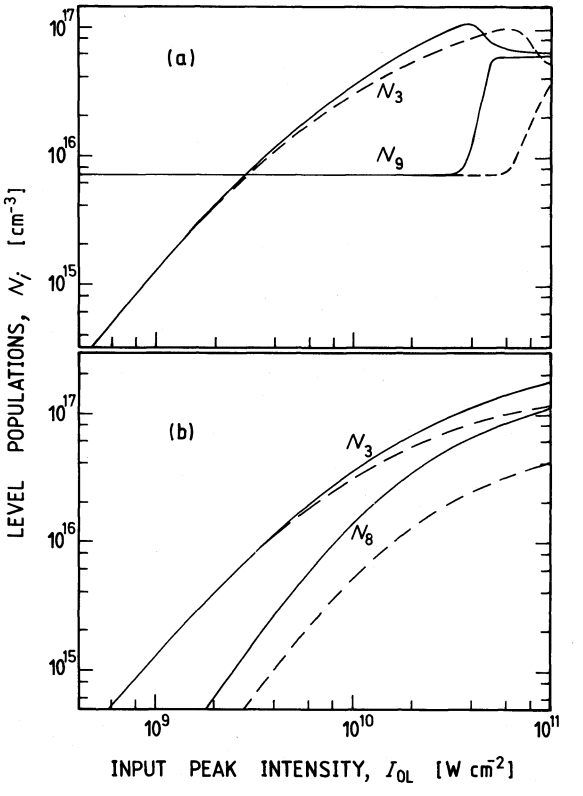

Figure 14 Level populations as a function of input pulse intensity in the middle of cell ($z = 1\,cm$). Time position $t = 0$, pump pulse duration $\Delta t = 30\,ps$. (a) Influence of S_0-state thermalization time τ_v on amplified spontaneous emission. Curves are for data of rhodamine B in methanol (Table I) except: $\sigma_{em} = 10^{-17}\,cm^2$, $\sigma_{ASE} = 6 \times 10^{-17}\,cm^2$, $\sigma_{ex,L} = \sigma_{ASE} = \sigma_{ex,ASE} = 0$, $\tau_v = 4\,ps$ (solid lines); $\sigma_{em} = 10^{-17}\,cm^2$, $\sigma_{ASE} = 6 \times 10^{-17}\,cm^2$, $\sigma_{ex,L} = \sigma_{ex,ASE} = 0$, $\tau_v = 1\,ps$ (dashed lines). (b) Influence of S_0-state thermalization time τ_v on stimulated emission at laser frequency ν_L. Curves are for data of rhodamine B in methanol (Table I) except: $\sigma_{em} = 10^{-17}\,cm^2$, $\sigma_{ASE} = \sigma_{ex,ASE} = \sigma_{ex,L} = 0$, $\tau_v = 4\,ps$ (solid lines); $\sigma_{em} = 10^{-17}\,cm^2$, $\sigma_{ASE} = \sigma_{ex,ASE} = \sigma_{ex,L} = 0$, $\tau_v = 1\,ps$ (dashed lines).

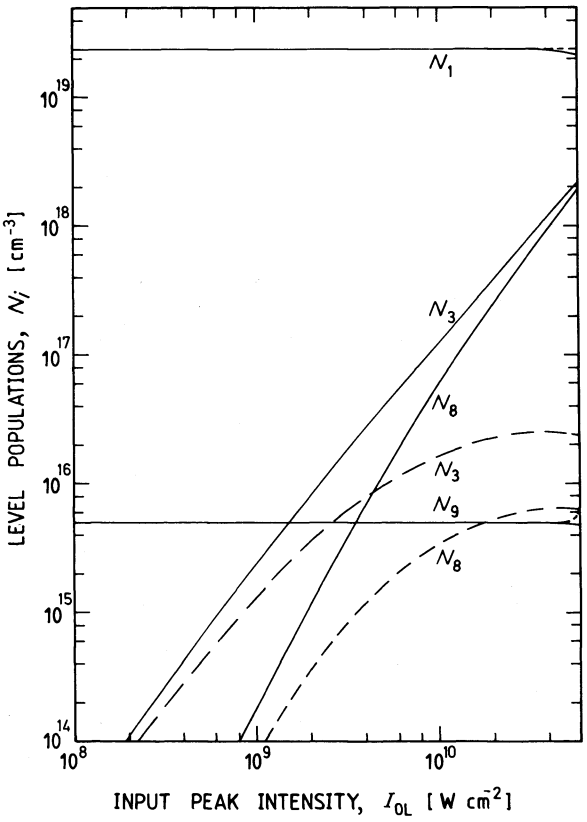

Figure 15 Level populations for rhodamine 6G in methanol. Time position $t = 0$, $\Delta t = 30$ ps. Best-fit data of Table I are used. Solid curves, cell entrance ($z = 0$); dashed curves, cell exit ($l = 2$ cm).

$\alpha = \sigma_{IM} N_{1'} + \sigma_{SCA} N_0$). The solution of Equation 21 is

$$I_L(l) = I_L(0) \frac{\exp(-\alpha l)}{1 + \frac{\sigma^{(2)} N_0}{h\nu_L \alpha} I_L(0)[1 - \exp(-\alpha l)]} \tag{22}$$

The energy transmission T_E is given by Equation 19. Using the best-fit parameters $\sigma^{(2)}$ of Table I, the energy transmissions give the same results as the solutions of the system of Equations 1 to 18 for $\sigma_{em} = \sigma_{ASE} = \sigma_{ex,L} = \sigma_{ex,ASE} = 0$ and $\tau_{IM} \to 0$ (no impurity bleaching). Using Equation 22 to fit the experimental points would underestimate the true $\sigma^{(2)}$ values by 30%.

The S_0 ground-state depopulation by two-photon absorption may be estimated by calculating the S_1-state population ($N_1 \simeq N_0 - N_3$). Three different situations are considered: (i) the S_1-state population declines by radiative and non-radiative decay (time constant τ_F); (ii) the S_1-state depopulation is dominated by stimulated emission at the pump laser frequency, ν_L; (iii) the S_1-state population is mainly reduced by amplified spontaneous emission.

(i) In the case of dominant S_1-state depopulation by spontaneous emission and nonradiative decay. Equation 3 reduces to

$$\frac{\partial N_3}{\partial t'} = \frac{\sigma^{(2)}(N_0 - N_3)}{2(h\nu_L)^2} I_L^2 - \frac{N_3}{\tau_F} \tag{23}$$

The first term describes the level population by two-photon absorption and fast relaxation from S_{n1} to S_1; the second term gives the relaxation from S_1 to S_0. Formal integration of Equation 23 leads

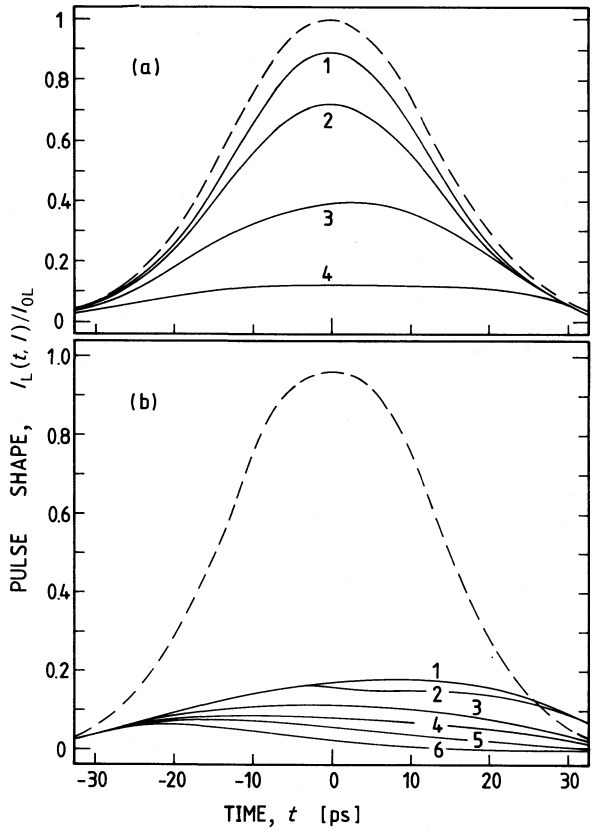

Figure 16 Pulse deformation by two-photon absorption dynamics. Dashed curves represent input pulse shapes. (a) Intensity dependent deformation. Solid curves belong to best-fit data of rhodamine 6G in methanol (Table I). The input peak intensities I_{0L} are (1) $1.5 \times 10^7\,W\,cm^{-2}$ (intensity reduction is due to linear losses), (2) $1 \times 10^9\,W\,cm^{-2}$, (3) $6 \times 10^9\,W\,cm^{-2}$, (4) $4 \times 10^{10}\,W\,cm^{-2}$. (b) Influence of various parameters on pulse shape. The curves belong to best-fit data of rhodamine B in acid methanol (Table I) at $I_{0L} = 4 \times 10^{10}\,W\,cm^{-2}$ except: (1) $\sigma_{em} = 10^{-17}\,cm^2$, $\sigma_{ASE} = \sigma_{ex,ASE} = \sigma_{ex,L} = 0$ (influence of stimulated emission); (2) $\sigma_{em} = 10^{-17}\,cm^2$, $\sigma_{ASE} = 6 \times 10^{-17}\,cm^2$, $\sigma_{ex,ASE} = \sigma_{ex,L} = 0$ (influence of amplified spontaneous emission); (3) $\sigma_{em} = \sigma_{ASE} = \sigma_{ex,ASE} = \sigma_{ex,L} = 0$; (4) $\sigma_{em} = \sigma_{ex,L} = 10^{-17}\,cm^2$, $\sigma_{ASE} - \sigma_{ex,ASE} \leqslant 0$; (5) $\sigma_{em} = \sigma_{ASE} = \sigma_{ex,ASE} = 0$, $\sigma_{ex,L} = 10^{-16}\,cm^2$ (influence of excited-state absorption); (6) $\sigma_{em} = 0$, $\sigma_{ex,L} = 10^{-16}\,cm^2$, $\sigma_{ASE} = 6 \times 10^{-17}\,cm^2$, $\sigma_{ex,ASE} = 0$ (combined effect of excited-state absorption and amplified spontaneous emission).

to

$$N_3(t' = t_0) = \frac{\sigma^{(2)}[N_0 - N_3(t_0)]\, I_{0L}^2\, t_{eff}}{2(h\nu_L)^2} \tag{24}$$

t_{eff} is approximately the minimum value of Δt_L and τ_F. Solving Equation 24 to $N_3(t_0)$ results in

$$\frac{N_3(t_0)}{N_0} = \left[1 + \frac{2(h\nu_L)^2}{\sigma^{(2)} I_{0L}^2\, t_{eff}}\right]^{-1} \tag{25}$$

Equation 25 indicates that for $I_{0L} \to \infty$ the S_1-state population tends to $N_3 \to N_0$. The saturation intensity $I_S^{(2)}$ for bleaching the ground-state population to $N_3/N_0 = 1/2$ (i.e. $N_3 = N_1 = N_0/2$) is

$$I_S^{(2)} = \frac{2^{1/2} h\nu_L}{[\sigma^{(2)} t_{eff}]^{1/2}} \tag{26}$$

These two-photon saturation intensities for rhodamine B and rhodamine 6G are included in Table I ($t_{eff} = \Delta t_L = 30\,ps$ is used).

(ii) If $\sigma_{em} - \sigma_{ex,L} > 0$, the stimulated emission limits the S_1-state population. Equation 3 reduces approximately to

$$\frac{\partial N_3}{\partial t'} = \frac{\sigma^{(2)}(N_0 - N_3)}{2(h\nu_L)^2} I_L^2 - \frac{\sigma_{em}(N_3 - N_8)}{h\nu_L} I_L - \frac{N_3}{\tau_F} \tag{27}$$

$\sigma_{ex,L}$ does not appear in Equation 27 because the molecules excited to level 5 are thought to relax immediately back to level 3. N_8 is given by Equation 8. The pumping of level 3 via two-photon

absorption and the depopulation of level 3 by stimulated emission are assumed to form an equilibrium within the pump pulse duration, i.e. $\partial N_3/\partial t = 0$ and $\partial N_8/\partial t = 0$. Under these conditions Equation 8 solves to

$$N_8 = \frac{\frac{\tau_v \sigma_{em} I_L}{h\nu_L} N_3 + \varrho_8 (N_0 - N_3)}{1 + \frac{\tau_v \sigma_{em} I_L}{h\nu_L}} \tag{28}$$

and Equation 27 gives

$$N_3 = N_0 \frac{\frac{\sigma^{(2)} I_L}{2h\nu_L} + \frac{\sigma_{em}\varrho_8}{1 + \tau_v \sigma_{em} I_L/h\nu_L}}{\frac{\sigma^{(2)} I_L}{2h\nu_L} + \frac{\sigma_{em}(1 + \varrho_8)}{1 + \tau_v \sigma_{em} I_L/h\nu_L} + \frac{h\nu_L}{\tau_F I_L}} \tag{29}$$

The filling of level 3 by two-photon absorption is lowered by the stimulated emission, which brings molecules back to the ground state. This effect reduces the effect of amplified spontaneous emission (see Fig. 9a). For $I_L \to \infty$, N_3 approaches N_0 because the two-photon absorption dominates at high intensities ($\sigma^{(2)} I_L > \sigma_{em}$ for high enough intensities). In case of $\sigma_{em} = 0$, Equation 29 reduces to Equation 25 with $t_{eff} = \tau_F$.

(iii) If amplified spontaneous emission becomes important the spontaneous fluorescence signal I_{sp} becomes exponentially amplified according to [27, 28]

$$I_{ASE} \approx I_{sp} \frac{\exp\left[(\sigma_{ASE} - \sigma_{ex,ASE}) N_3 l\right] - 1}{(\sigma_{ASE} - \sigma_{ex,ASE}) N_3 l} \tag{30}$$

For a crude estimate I_{ASE} is thought to approach the absorbed pump-pulse intensity when $I_{ASE}/I_{sp} \simeq \exp(12)$. This amplification is achieved for

$$N_3 \approx \frac{15}{(\sigma_{ASE} - \sigma_{ex,ASE}) l} \tag{31}$$

Equation 31 gives an upper limit for the S_1-state population, and $N_1 = N_0 - N_3$ gives the minimal ground-state population.

If the limited N_3-value due to amplified spontaneous emission is small compared to N_3 of Equation 29, then the effect of stimulated emission at the pump-laser frequency is weakened.

7. Conclusions

The two-photon absorption dynamics of picosecond ruby laser pulses in rhodamine B and rhodamine 6G have been studied and the two-photon-absorption and excited-state-absorption cross-sections involved have been measured. The influence of excited-state absorption, stimulated emission, and amplified spontaneous emission on the pump-pulse transmission, temporal pump-pulse deformation and the dye level population has been investigated. The theoretical discussion has considered, in general, the dynamics of two-photon absorption, including various absorption, emission and relaxation processes.

Acknowledgements

The authors thank M. Weidner for experimental assistance during part of the measurements and Th. Ascherl for technical assistance. They also thank the Rechenzentrum of the University for the allocation of computer time, and the Deutsche Forschungsgemeinschaft for financial support.

References

1. F. P. SCHÄFER and W. SCHMIDT, *IEEE J. Quantum Electron.* **QE-2** (1966) 357.
2. D. J. BRADLEY, M. H. R. HUTCHINSON and H. KOETSER, *Proc. R. Soc.* **A329** (1972) 105.

3. J. P. HERMANN and J. DUCUING, *Opt. Commun.* **6** (1972) 101.
4. E. B. ASLANIDI and E. A. TIKHONOV, *Opt. Spectrosc.* **37** (1974) 446.
5. J. KRASINSKI, W. MAJEWSKI and M. GLÓDŻ, *Opt. Commun.* **14** (1975) 187.
6. B. FOUCAULT and J. P. HERMANN, *ibid.* **15** (1975) 412.
7. L. PARMA and N. OMENETTO, *Chem. Phys. Lett.* **54** (1978) 541.
8. J. A. GIORDMAINE, P. M. RENTZEPIS, S. L. SHAPIRO and K. W. WECHT, *Appl. Phys. Lett.* **11** (1967) 216.
9. W. RAPP and B. GRONAU, *Chem. Phys. Lett.* **8** (1971) 529.
10. A. N. RUBINOV, M. C. RICHARDSON, K. SALA and A. J. ALCOCK, *Appl. Phys. Lett.* **27** (1975) 358.
11. D. J. BRADLEY, T. MORROW and M. S. PETTY, *Opt. Commun.* **6** (1972) 394.
12. R. PARETTI and P. RANSON, *ibid.* **3** (1971) 62.
13. D. J. BRADLEY, M. H. R. HUTCHINSON, H. KOETSER, T. MORROW, G. H. C. NEW and M. S. PETTY, *Proc. R. Soc.* **A328** (1972) 97.
14. S. MORY, D. LEUPOLD and R. KÖNIG, *Opt. Commun.* **6** (1972) 394.
15. J. HERRMANN, M. PALME and K. E. SÜSSE, *Opt. Quantum Electron.* **10** (1978) 195.
16. S. J. STRICKLER and R. A. BERG, *J. Chem. Phys.* **37** (1962) 814.
17. D. RICARD and J. DUCUING, *J. Chem. Phys.* **62** (1975) 3616.
18. A. SEILMEIER, P. O. J. SCHERER and W. KAISER, *Chem. Phys. Lett.* **105** (1984) 140.
19. D. N. DEMPSTER, *J. Photochem.* **2** (1973) 343.
20. B. G. HUTH, G. I. FARMER and M. R. KAGEN, *J. Appl. Phys.* **40** (1969) 5145.
21. W. BLAU, W. DANKESREITER and A. PENZKOFER, *Chem. Phys.* **85** (1984) 473.
22. A. PENZKOFER and P. SPERBER, *ibid.* **88** (1984) 309.
23. N. I. KUNAVIN, R. N. NURRUKHAMETOV and G. T. KHACHATUROVA, *Sov. J. Appl. Spectrosc.* **26** (1977) 735.
24. Y. LU and A. PENZKOFER, *Chem. Phys.* **107** (1986) 175.
25. A. PENZKOFER and Y. LU, *ibid.* **103** (1986) 399.
26. W. M. McCLAIN, *Acc. Chem. Res.* **7** (1974) 129.
27. A. PENZKOFER and W. FALKENSTEIN, *Chem. Phys. Lett.* **44** (1976) 547.
28. A. PENZKOFER and W. BLAU, *Opt. Quantum Electron.* **15** (1983) 325.
29. Th. FÖRSTER, *Z. Naturforsch.* **4a** (1949) 321.
30. K. H. DREXHAGE, *Laser Focus* **9**(3) (1973) 35.
31. O. G. PETERSON, J. P. WEBB, W. C. McCOLGIN and J. E. EBERLY, *J. Appl. Phys.* **42** (1971) 1917.
32. M. J. WEBER and M. BASS, *IEEE J. Quantum Electron.* **5** (1969) 175.
33. B. B. SNAVELY, in 'Photophysics of Aromatic Molecules', edited by J. B. Birks (Wiley, London, 1973) p. 239.
34. P. R. HAMMOND, *IEEE J. Quantum Electron.* **QE-15** (1979) 624.
35. *Idem, ibid.* **QE-16** (1980) 1157.
36. J. WIEDMANN and A. PENZKOFER, *Nuovo Cimento* **63B** (1981) 459.
37. W. BLAU and A. PENZKOFER, *Opt. Commun.* **36** (1981) 419.
38. A. PENZKOFER, *Opto-Electronics* **6** (1974) 87.
39. A. PENZKOFER and W. FALKENSTEIN, *Opt. Quantum Electron.* **10** (1978) 399.
40. W. FALKENSTEIN, A. PENZKOFER and W. KAISER, *Opt. Commun.* **27** (1978) 151.
41. M. D. GALANIN and S. A. TSCHISCHKOWA, *Kratk. Soobshch. Fiz.* **4** (1971) 35.
42. I. KAPLAN and J. JORTNER, *J. Chem. Phys.* **32** (1978) 381.
43. A. V. ARISTOV and Yu. S. MASLYUKOV, *Opt. Spectrosc.* **41** (1976) 141.
44. D. W. PHILLION, *Appl. Phys. Lett.* **27** (1975) 85.
45. K. A. SELANGER, J. FALNES and T. SIKKELAND, *J. Phys. Chem.* **81** (1977) 1960.